Journal of Materials Chemistry C

ROYAL SOCIETY OF CHEMISTRY

PAPER

View Article Online
View Journal | View Issue

Cite this: J. Mater. Chem. C, 2020, 8, 5535

Polymer field-effect transistor memory based on a ferroelectric nylon gate insulator†

Saleem Anwar,‡[ab] Beomjin Jeong,‡[a] Mohammad Mahdi Abolhasani,[ac] Wojciech Zajaczkowski,[a] Morteza Hassanpour Amiri[a] and Kamal Asadi *[a]

Received 16th December 2019,
Accepted 23rd February 2020

DOI: 10.1039/c9tc06868f

rsc.li/materials-c

Nylons are one of the most successful commercialized polymers and can also be made to have ferroelectric properties. However, use of nylons in microelectronic devices like ferroelectric field-effect transistors has proven to be challenging due to the difficulty in achieving ferroelectric thin films by solution processing. In this work, we present ferroelectric field-effect transistor (FeFET) memory with a ferroelectric nylon-11 gate. Water quenching allows for the fabrication of ultra-smooth ferroelectric nylon-11 thin films. A bottom-gate top-contact (BGTC) FeFET is successfully demonstrated with a p-type semiconducting polymer, poly(triaryl amine) (PTAA), as a channel. The nylon-11 FeFET shows reliable memory functionality. The demonstration of nylon-11 based FeFETs makes nylons a promising material for applications in organic electronics, such as flexible devices, electronic textiles and biomedical devices.

Introduction

Data storage devices are key components for upcoming wearable electronics, which requires mechanically flexible materials with reliable electrical memory operation. Ferroelectric polymers have been of great interest owing to their bistable electrical polarization state that gives rise to memory functionality.[1] Memory elements based on diodes,[2] capacitors,[3] and flexible and even foldable field-effect transistors (FET)[4–9] have been demonstrated, using mainly poly(vinylidene fluoride) (PVDF) and its copolymer of poly(vinylidene fluoride-*co*-trifluoroethylene) (P(VDF–TrFE)). Despite the availability of various ferroelectric polymers, research is mainly focused on fluoropolymers due to (i) ease of processing into thin films and (ii) ease of achieving the ferroelectric crystalline phase in thin films upon solution processing.[10]

Polyamides, or nylons, are one of the most successful commercialized polymers and are extensively used in textiles and structural and high performance applications. The polymer chain in nylons is composed of amide units that are separated by CH_2 units. Odd nylons that have an even number of CH_2 units between the amide bonds exhibit ferroelectric properties *i.e.* remanent polarization, P_r, and coercive field, E_c, that are on par with fluorinated polymers.[11] Despite their significant potential, microelectronic devices employing odd nylons have rarely been demonstrated, mainly because of the difficulty in thin film fabrication of ferroelectric nylons. The exploitation of ferroelectric odd-nylons is hindered due to difficulties associated with (i) solution processing of nylons into thin films, and (ii) arriving at the crystalline ferroelectric δ′-phase, which is characterized by a metastable mesophase with randomly oriented hydrogen bonds along the backbone and between the adjacent chains.[12–14]

Solution processing of nylon thin films is challenging because of the excellent solvent resistance of nylons to most common organic solvents. Thin films processed from the limited number of applicable solvents such as formic acid, *m*-cresol, or trifluoroacetic acid (TFA)[15,16] produce films with porous structure, which is unsuitable for microelectronic applications.[17–19] A previous attempt to develop a nylon-11 gate insulator using a high boiling point solvent, *m*-cresol, has resulted in poor memory operation of the resulting FeFETs due to the uncontrolled high roughness of the nylon-11 film.[20] Therefore, nylon-based functional microelectronic devices such as ferroelectric field effect transistors (FeFETs) have hardly been realized.

Recently, we have demonstrated ferroelectricity in solution processed thin films of odd-nylons using a solvent mixture of TFA : acetone [60 : 40 mole percent (mol%)].[21] The ferroelectric phase is realized by placing the wet spin-coated film in a vacuum chamber to quickly extract the solvent and provide fast crystallization conditions. The resulting vacuum-quenched thin films show small crystallites and the absence of spherulitic

[a] Max Planck Institute for Polymer Research, Ackermannweg 10, 55128 Mainz, Germany. E-mail: asadi@mpip-mainz.mpg.de
[b] School of Chemical & Materials Engineering, National University of Sciences & Technology, Sector H–12, Islamabad, Pakistan
[c] Chemical Engineering Department, University of Kashan, 8731753153, Kashan, Iran

† Electronic supplementary information (ESI) available. See DOI: 10.1039/c9tc06868f
‡ These authors contributed equally to this work.

superstructures. The solvent-quenching process using a vacuum, to some degree, imitates the supercooling process from a melt, which is known to yield the pseudohexagonal non-spherulitic δ′-phase.[21] However, thin films produced by vacuum quenching have a roughness of around 5 nm, which is not suited for applications in devices such as FeFETs.[22] We hypothesize that the roughness is due to the extended solvent-quenching time, since the vacuum is not strong enough to quickly extract solvent molecules. To exactly imitate supercooling, the solvent extraction process should be done much quicker. The δ′-phase crystallites are then much smaller and the film roughness would reduce, rendering nylon-11 suitable for FeFET applications.

Here, we report FeFETs based on ultra-smooth nylon-11 thin films that are realized by a solvent quenching method using a non-solvent, water. The resulting nylon-11 films are non-porous and show dielectric and ferroelectric properties similar to the vacuum-quenched ones. The resultant nylon FeFETs show excellent memory functionality with a high ON–OFF ratio, good retention time and excellent cycle endurance. Our demonstration of nylon FeFETs offers a great opportunity for technological utilization of nylons in microelectronics.

Experimental

Materials

Nylon-11 was purchased from Sigma Aldrich. TFA and acetone (99.8%, extra dry) were purchased from Carl Roth GmbH and Acros Organics, respectively. PTAA was purchased from Merck. All materials were used as received.

Preparation of nylon-11 thin films

Nylon-11 was dissolved in a TFA : acetone mixture (60 : 40 mol%) with a concentration of 35 mg ml^{-1}. Thin films were fabricated by spin-coating the solution on glass substrates for one minute at 1000 rpm, followed by placing the substrate either in a vacuum desiccator (vacuum quenching) for 15 minutes or in a deionized water bath (water quenching) for 5 s. The thickness of the nylon-11 thin films was around 300 nm.

Device fabrication

To fabricate ferroelectric capacitors, 50 nm Au bottom electrodes with a 1 nm Cr adhesion layer were thermally evaporated using a shadow mask on glass substrates. After forming nylon-11 thin films, a Au top electrode (50 nm) was deposited using a shadow mask to form a crossbar pattern with a capacitor area of 0.0016 cm^2. A bottom gate, top contact (BGTC) transistor was fabricated on the glass substrate. For the gate electrode, Cr (1 nm) and Au (50 nm) were deposited by thermal evaporation with a predefined shadow mask. The nylon-11 gate dielectric was formed on the gate electrode by water quenching. PTAA was dissolved in toluene (1 wt%) and spin-coated on top of a nylon film at 1000 rpm for 60 s to form a 70 nm layer. 30 nm of Au was thermally evaporated onto the PTAA–nylon stack through a shadow mask, defining the source and drain electrodes with a channel length of 20 μm. The as-fabricated FeFETs were heated at 80 °C for 2 hours in a vacuum oven to remove traces of residual solvents.

Structural characterization

The surface morphology of the resulting thin films was inspected by atomic force microscopy (AFM) (Nanoscope Dimension 3100 Bruker). Wide-angle X-ray diffraction (WAXD) measurements of the films were performed at the DELTA synchrotron using beamline BL09 with a photon energy of 13 keV (λ = 0.9537 Å). The beam size was 1.0 mm × 0.2 mm (width × height), and samples were irradiated just below the critical angle for total reflection with respect to the incoming X-ray beam ($\sim$0.1°). The diffraction intensity was detected on a 2-D image plate (MAR-345) with a pixel size of 150 μm (2300 × 2300 pixels), and the detector was placed 523 mm from the sample center. Diffraction data are expressed as a function of the diffraction vector: $q = 4\pi/\lambda \sin(\Theta)$, where Θ is half the diffraction angle and λ = 0.9537 Å is the wavelength of the incident radiation. All X-ray measurements were performed under a vacuum ($\sim$1 mbar) to reduce air scattering and beam damage to the sample.

Electrical measurements

Ferroelectric capacitors were characterized in a vacuum probe station at 10^{-5} mbar. The *D–E* hysteresis loops were measured using a Radiant precision multiferroic test system (Radiant Technologies, Inc.). Data retention and polarization fatigue tests were performed using the same setup. For data retention, a write pulse was followed by two read pulses of the same amplitude but opposite direction. All pulse widths were fixed at 10 ms. The fatigue test was performed using a continuous triangular waveform with an amplitude of 250 MV m^{-1}. After a predefined number of cycles, the remanent polarization was determined by PUND measurements using 10 ms wide pulses. Impedance measurements were performed as well in a vacuum at 10^{-5} mbar, using a Novocontrol analyser. Electrical measurements of the FeFETs were carried out in a vacuum with a Keithley 4200-SCS instrument. The retention of the ON- and OFF current at V_{GS} = 0 V was measured after a single-sweep of VGS from 0 V to −50 V (programming) and +50 V (erasing), respectively. The switching cycle was measured after pulsing −50 V and +50 V for 100 ms to set the FeFET in the ON and OFF states, respectively.

Results and discussion

Fig. 1a and b present AFM height and phase images, respectively, for the reference nylon-11 thin film quenched in a vacuum. The film is composed of small crystallites and does not show spherulitic microstructure. The film is optically transparent, but the mean RMS roughness is around 5 nm. The water-quenched thin film, Fig. 1c and d, shows non-spherulitic morphology, the same as the one of the vacuum-quenched films. However, the water-quenched thin films show remarkably low RMS roughness values around 2 nm.

For solvents that are miscible with water, placing the solvent-wet film in a water bath leads to liquid–liquid (L–L) demixing, resulting in polymer-rich and polymer-poor phases.

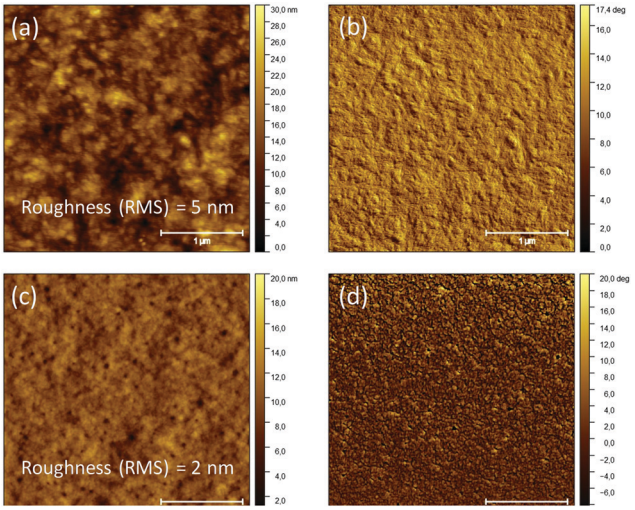

Fig. 1 Tapping mode AFM height and phase images, respectively, of a nylon-11 thin film obtained by (a and b) vacuum quenching and (c and d) water quenching.

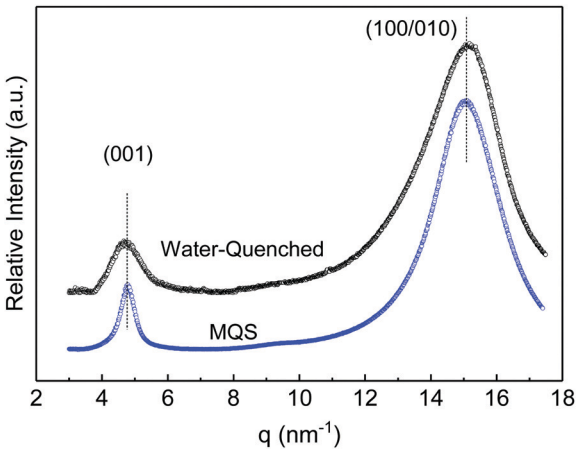

Fig. 2 WAXD pattern for the water-quenched thin film compared with a melt-quenched stretched thick film.

As a result, a porous and rough morphology is obtained for the solidified film. From this point of view, achieving ultra-smooth nylon-11 thin-films is counterintuitive because TFA:acetone is miscible with water. However, L–L demixing does not seem to play a role during the water-quenching process. Here we tentatively explain the film formation mechanism. TFA is a strong acid, which by protonating the amide bond weakens the hydrogen bonds and solubilizes nylon-11. Addition of acetone (by 40 to 50 mol%) increases the acidity due to the deshielding of the acidic proton.[21] On the other hand, water has a strong tendency to dissociate a proton from TFA:acetone and to form hydronium ions (H_3O^+). The formation of H_3O^+ deprotonates the amides along the polymer chains, leading to solidification of the nylon-11 film. The kinetics of H_3O^+ formation is much faster than the L–L demixing, such that before L–L demixing sets in, all the solvent molecules are depleted from the film. To support this claim, a mixture of TFA : acetone (60 : 40 mol%) with water (50 : 50 mol%) has been prepared. In sharp contrast with TFA:acetone, the mixture with water does not dissolve nylon-11, as shown in Fig. S1 (ESI†), under the same room-temperature conditions. The mixing with water renders TFA:acetone a non-solvent for nylon-11, due to the unavailability of protons to attack hydrogen bonded amides.

Crystallization at high solvent depletion rates is governed by homogeneous nucleation, where the number of nucleation sites upon solidification is several orders of magnitude larger in comparison with crystallization at low solvent depletion rates, such as conventional spin coating. Due to the large number of crystallites, lateral growth of crystalline lamellae into spherulites is hindered, and therefore the ferroelectric δ′-phase is obtained.[21,23] The quick depletion of TFA:acetone from the film mimics supercooling of nylon-11 from melts, which yields the crystalline ferroelectric δ′-phase.[21] Fig. 2 shows the WAXD patterns of the water-quenched thin film and, as a reference, that of the melt-quenched-stretched (MQS) thick film. The MQS film shows the (001) diffraction peak at 4.79 nm^{-1}, corresponding to a *d*-spacing of 1.311 nm in perfect agreement with the literature values of the δ′-phase.[13,24–26] The (001) reflection gives the length of repeat units in the crystalline structure along the polymer chain. A second diffraction peak at 15.10 nm^{-1} (a *d*-spacing of 0.416 nm) is a superposition of the (100) and (010) peaks and gives the inter-chain distance along the hydrogen bonds and the inter-sheet distance between the hydrogen bonded sheets, respectively. The presence of a single diffraction peak around 15 nm^{-1} indicates the low inter-molecular arrangement of the chains with random orientation of hydrogen bonds along the backbone and between adjacent chains.[13,14]

The diffraction peaks of the water-quenched thin film show similar reflections to those of the MQS thick film, as well as the vacuum quenched one.[21] The (001) and (100/010) reflection peaks for the water-quenched thin film are exactly at the same position. Therefore, the WAXD measurement unambiguously indicates that water quenching allows one to readily produce thin films of nylon-11 with the ferroelectric δ′-phase.

The electrical displacement (*D*) *vs.* electrical field (*E*) hysteresis loops (top) and switching current (bottom) of the reference vacuum-quenched and the water-quenched capacitors are given in Fig. 3a. P_r and E_c of both samples are 4.5 ± 0.2 μC cm^{-2} and 200 ± 10 MV m^{-1}, respectively, and are similar to literature values, indicating the effectiveness of the water quenching process.[11,13,14,27] To show the robustness and applicability of the films for microelectronic applications, we have measured the retention time of the polarization and cycle endurance as shown in Fig. 3b. The capacitor does not show any sign of depolarization, and P_r remains stable for nearly 10^5 seconds. Moreover, the water-quenched thin films show excellent performance upon repeated polarization switching processes, and the polarization is stable for more than one million switching cycles. A slight increase in the P_r value is observed upon cycling, which is attributed to electric field induced polarization or electroforming.[28,29] It has been shown that nylon-11 films show fatigue-free performance that can even exceed that of PVDF and P(VDF–TrFE) capacitors.[28]

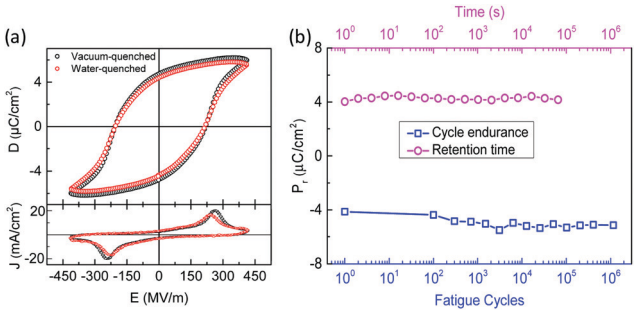

Fig. 3 (a) *D*–*E* ferroelectric hysteresis loop (top) and switching current (bottom) of vacuum- and water-quenched thin films represented as black and red circles, respectively, and (b) cycle endurance and polarization retention of the water-quenched film.

We note that nylons are known for their water uptake. The presence of water molecules inside the film would jeopardize the ferroelectric performance of the nylon-11 capacitor. To investigate whether water uptake takes place during water quenching, we have studied the dielectric response of the nylon-11 thin films. Fig. 4 shows the relative permittivity ε' (top) and loss ε'' (bottom) spectra of both the vacuum- and water-quenched samples. ε' or the dielectric constant exhibits a very weak frequency dependence at the low frequency limit (<1 Hz), which is about 4 and reduces to 3.5 at 1 MHz. The lack of strong frequency dependence particularly at low frequencies could be assigned to the lack of ions (water or solvent molecules) in the films. The loss for both films is about the same and again shows only weak frequency dependence. The impedance spectra indicate a lack of ions, including water molecules, in both films, in particular in the water-quenched nylon-11 film. Therefore, the water quenching process has no effect on the performance of the nylon-11 capacitors and does not hinder the application of nylon-11 for microelectronic devices.

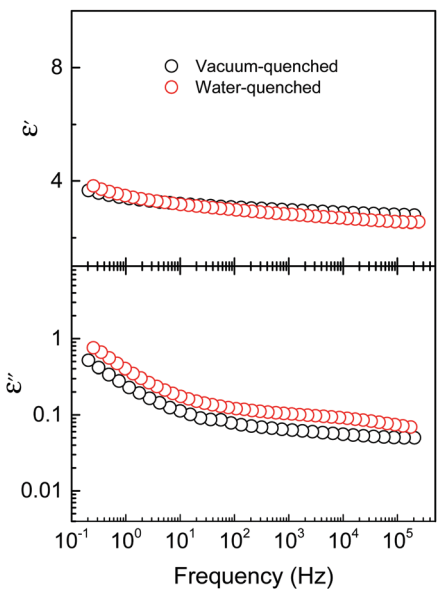

Fig. 4 Frequency dependence of the relative permittivity (ε') (top) and loss (ε'') (bottom) of the nylon-11 thin film processed *via* vacuum quenching (black) and water quenching (red).

Achieving low roughness with minimized dielectric losses renders water-quenched nylon-11 thin films suitable for a gate insulator in FeFETs. To that end, nylon-11 FeFETs with BGTC architecture and p-type semiconductor polytriarylamide, PTAA, have been fabricated. The device schematic and chemical structure of PTAA are shown in Fig. 5a. The p-type PTAA FeFET exhibits large hysteresis in the I_{DS}–V_{GS} transfer characteristic, arising from the ferroelectric polarization of the nylon-11 gate as shown in Fig. 5b. Upon application of a negative gate bias, holes in PTAA accumulate at the interface between nylon-11 and PTAA. The coercive gate bias at which the nylon-11 polarizes is about −30 V. The negative polarization of nylon-11 is compensated by hole carriers in PTAA, giving rise to a significant increase in channel conductance (ON-state). When the positive gate voltage is biased above +30 V, nylon-11 reverses polarization. The positively polarized nylon-11 ferroelectric at the interface with PTAA cannot be compensated and the ferroelectric is depolarized, and thus the channel becomes depleted (OFF-state).[30] The nylon-11 FeFET has bistable current states at zero gate bias with an ON–OFF ratio that is larger than 10^3 and operates as a ferroelectric memory. A gate current level of 10^{-8} A was observed at programming and erasing voltages. We note that microelectronic devices are typically encapsulated against ambient conditions for operational stability. Therefore, water uptake in nylon-11 will not be of concern in applications when the devices are properly encapsulated.

The data retention and cycle endurance of the nylon-11 FeFET are presented in Fig. 5c and d. The ON- and OFF-states are programmed by applying −50 V and +50 V gate bias, respectively, and then the channel conductance is probed at 0 V gate bias. The current for both the ON- and OFF-states has remained constant in time and remained around 10^{-7} and 10^{-10} A, respectively, as shown

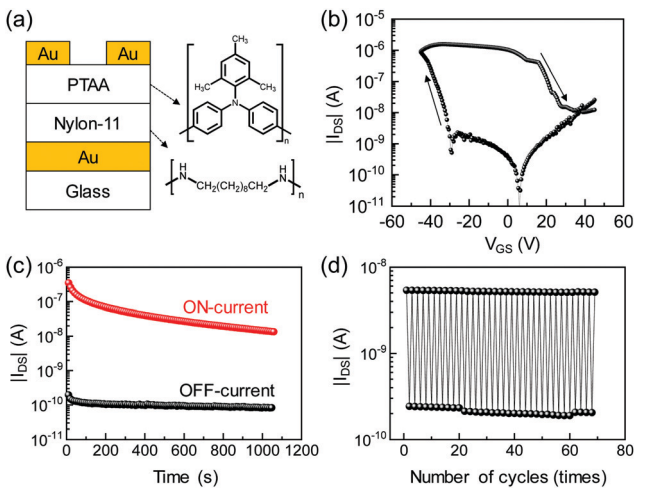

Fig. 5 (a) A schematic of the BGTC FeFET with the nylon ferroelectric gate insulator. Chemical structures of the materials used are provided. (b) A transfer characteristic of the FeFET with a nylon ferroelectric gate. The ferroelectric layer thickness was 300 nm. The sweeping direction represented by the arrow shows ferroelectric switching and resultant hysteresis. (c) Data retention with time and (d) cycle endurance of the FeFET programmed at −50 V for ON-current and erased at +50 V for OFF-current. The read voltage was 0 V.

in Fig. 5c. We have demonstrated, in Fig. 3b, superior polarization stability of nylon-11 in time. Therefore, long term stability of the ON-state for the PTAA based FeFET is expected due to the presence of the compensation charges. The slight reduction in the ON-state current however could originate from the aging of the PTAA since organic semiconductors are known to be prone to degradation under electrical biasing.[31] The cycle endurance of the nylon-11 FeFET is explored for repetitive data programing and erasing cycles. Fig. 5d shows the current level in the PTAA channel at a read gate voltage of V_{GS} = 0 V repetitively changed upon programming at V_{GS} = −50 V (ON-state) and erasing at V_{GS} = +50 V (OFF-state). The ON–OFF ratio of the PTAA channel current remained around 30 after switching over 60 times. The switching time for the nylon-11 FeFET is set to 100 ms to provide a longer time for polarization at a switching field of 167 MV m^{-1} (V_{GS} = 50 V), which is lower than the 250 MV m^{-1} used in the capacitor. We note that nylon-11 has shown excellent endurance under repetitive polarization switching cycles for more than 10^6 cycles (Fig. 3b). Therefore, upon further switching of the nylon-11 gate, the same ON/OFF ratio is expected.

Conclusions

We have successfully demonstrated that water quenching produces ultra-smooth and pinhole-free ferroelectric nylon-11 films of sub-micron thickness with a low dielectric loss. The resultant nylon-11 film has been applied as a gate insulator in BGTC thin film transistors. The ferroelectric nylon gate has allowed us to develop a p-type polymer-based FeFET memory with PTAA as a semiconducting polymer channel. The FeFET has shown a high ON–OFF ratio, good data retention time, and reliable cycle endurance. Our results suggest that commercially available, easily synthesized, and cost-effective nylon can be fully exploited in microelectronic devices like in thin film transistors and memory.

Conflicts of interest

There are no conflicts to declare.

Acknowledgements

B. J. and M. M. A. would like to thank the Alexander von Humboldt Foundation for their financial support. S. A. thanks the National University of Science and Technology (Pakistan) for the financial support. K. A. and M. H. A. acknowledge the Alexander von Humboldt Foundation for the funding provided in the framework of the Sofja Kovalevskaja Award, endowed by the Federal Ministry of Education and Research, Germany and the Max-Planck Institute for Polymer Research for technical support. Open Access funding provided by the Max Planck Society.

References

1 R. C. G. Naber, K. Asadi, P. W. M. Blom, D. M. de Leeuw and B. de Boer, *Adv. Mater.*, 2010, **22**, 933.
2 M. Kumar, H. S. Dehsari, S. Anwar and K. Asadi, *Appl. Phys. Lett.*, 2018, **112**, 123302.
3 K. Asadi, M. Li, P. W. Blom, M. Kemerink and D. M. de Leeuw, *Mater. Today*, 2011, **14**, 592.
4 R. C. Naber, C. Tanase, P. W. Blom, G. H. Gelinck, A. W. Marsman, F. J. Touwslager, S. Setayesh and D. M. De Leeuw, *Nat. Mater.*, 2005, **4**, 243.
5 A. K. Tripathi, A. J. Van Breemen, J. Shen, Q. Gao, M. G. Ivan, K. Reimann, E. R. Meinders and G. H. Gelinck, *Adv. Mater.*, 2011, **23**, 4146.
6 K. L. Kim, W. Lee, S. K. Hwang, S. H. Joo, S. M. Cho, G. Song, S. H. Cho, B. Jeong, I. Hwang, J.-H. Ahn, Y.-J. Yu, T. J. Shin, S. K. Kwak, S. J. Kang and C. Park, *Nano Lett.*, 2015, **16**, 334.
7 M. Khan, U. S. Bhansali and H. N. Alshareef, *Adv. Mater.*, 2012, **24**, 2165.
8 R. H. Kim, H. J. Kim, I. Bae, S. K. Hwang, D. B. Velusamy, S. M. Cho, K. Takaishi, T. Muto, D. Hashizume, M. Uchiyama, P. André, F. Mathevet, B. Heinrich, T. Aoyama, D.-E. Kim, H. Lee, J.-C. Ribierre and C. Park, *Nat. Commun.*, 2014, **5**, 3583.
9 K. Asadi, P. W. Blom and D. M. de Leeuw, *Appl. Phys. Lett.*, 2011, **99**, 156.
10 H. Zhu, S. Yamamoto, J. Matsui, T. Miyashita and M. Mitsuishi, *RSC Adv.*, 2016, **6**, 32007.
11 B. Mei, J. Scheinbeim and B. Newman, *Ferroelectrics*, 1993, **144**, 51.
12 V. Gelfandbein and D. Katz, *Ferroelectrics*, 1981, **33**, 111.
13 Z. Zhang, M. H. Litt and L. Zhu, *Macromolecules*, 2016, **49**, 3070.
14 Z. Zhang, M. H. Litt and L. Zhu, *Macromolecules*, 2017, **50**, 5816.
15 M. Jabbari, M. Skrifvars, D. Åkesson and M. J. Taherzadeh, *Int. J. Polym. Sci.*, 2018, **9**, 6235165.
16 K. Behler, M. Havel and Y. Gogotsi, *Polymer*, 2007, **48**, 6617.
17 E. L. Papadopoulou, F. Pignatelli, S. Marras, L. Marini, A. Davis, A. Athanassiou and I. S. Bayer, *RSC Adv.*, 2016, **6**, 6823.
18 M. Li, I. Katsouras, C. Piliego, G. Glasser, I. Lieberwirth, P. W. Blom and D. M. de Leeuw, *J. Mater. Chem. C*, 2013, **1**, 7695.
19 H. S. Dehsari, J. J. Michels and K. Asadi, *J. Mater. Chem. C*, 2017, **5**, 10490.
20 H. Sakai, H. Isoda and Y. Furukawa, *Jpn. J. Appl. Phys.*, 2012, **51**, 040210.
21 S. Anwar, D. Pinkal, W. Zajaczkowski, P. V. Tiedemann, H. S. Dehsari, M. Kumar, T. Lenz, U. Kemmer-Jonas, W. Pisula, M. Wagner, R. Graf, H. Frey and K. Asadi, *Sci. Adv.*, 2019, **5**, eaav3489.
22 S. E. Fritz, T. W. Kelley and C. D. Frisbie, *J. Phys. Chem. B*, 2005, **109**, 10574.
23 A. Mollova, R. Androsch, D. Mileva, C. Schick and A. Benhamida, *Macromolecules*, 2013, **46**, 828.
24 J. T. Jung, J. F. Kim, H. H. Wang, E. Di Nicolo, E. Drioli and Y. M. Lee, *J. Membr. Sci.*, 2016, **514**, 250.
25 L. Chocinski-Arnault, V. Gaudefroy, J. Gacougnolle and A. Riviere, *J. Macromol. Sci., Part B: Phys.*, 2002, **41**, 777.

26 S. S. Nair, C. Ramesh and K. Tashiro, *Macromolecules*, 2006, **39**, 2841.
27 J. Lee, Y. Takase, B. Newman and J. Scheinbeim, *J. Polym. Sci., Part B: Polym. Phys.*, 1991, **29**, 273.
28 D. Zhao, I. Katsouras, M. Li, K. Asadi, J. Tsurumi, G. Glasser, J. Takeya, P. W. M. Blom and D. M. de Leeuw, *Sci. Rep.*, 2014, **4**, 5075.
29 P. von Tiedemann, S. Anwar, U. Kemmer-Jonas, K. Asadi and H. Frey, *Macromol. Chem. Phys.*, 2020, **221**, 1900468.
30 R. Naber, J. Massolt, M. Spijkman, K. Asadi, P. Blom and D. De Leeuw, *Appl. Phys. Lett.*, 2007, **90**, 113509.
31 Q. Niu, R. Rohloff, G.-J. A. H. Wetzelaer, P. W. M. Blom and N. I. Crăciun, *Nat. Mater.*, 2018, **17**, 557.